Approximation-Free Prespecified Time Bionic Reliable Control for Vehicle Suspension

Tenglong Huang, *Graduate Student Member, IEEE*, Jue Wang, and Huihui Pan, *Senior Member, IEEE*

***Abstract*— Developing a solution to suppress vibration with low energy consumption is an interesting and significant topic for vehicle suspension. This paper proposes an approximation-free prespecified time energy-efficient fault-tolerant control scheme for active suspensions. Inspired by the X-shaped asymmetric structures that existed in animal limbs, the energy consumption can be significantly reduced, without changing the hardware structure and optimization, only by introducing bionic dynamics. Moreover, the states can converge to a neighborhood of zero within a pre-specified finite time interval by employing the designed bionic control framework. Note that the settling time is independent of the initial values of states and the controller parameters. Meanwhile, system uncertainties, external perturbations, and actuator faults can be handled effectively by the presented approximation-free controller. The knowledge of actuator faults, perturbation, and suspension model is not required for controller design. By using the designed approximation-free prespecified time bionic fault-tolerant controller, excellent ride comfort can be achieved with low energy consumption. Experiments are performed and corresponding comparison results are provided to demonstrate the superiority of the developed control method.**

***Note to Practitioners*—Vehicle active suspensions offer a higher degree of control freedom to isolate vibrations, however, are associated with expensive energy consumption. Model uncertainties, non-linearities, external disturbances, and actuator faults in real-world environments can lead to performance degradation. Motivated by this, this paper designs a bio-inspired energy-saving prespecified time approximation-free fault-tolerant controller. By employing dynamical properties inspired by X-type structures that exist in animal limbs or bones, efficient energy-saving control can be achieved. The transient responses are constrained to a prescribed region and converge to a given steady-state region within a pre-assigned time. The proposed controller does not require approximation structures such as neural networks or fuzzy rules. Consequently, the controller exhibits a simple structure that can be readily implemented and deployed in practical suspension systems. Experimental results obtained from practical suspension platforms under different road excitations demonstrate satisfactory energy saving and vibration suppression performance of the presented control scheme.**

***Index Terms*— Energy consumption, prespecified time, bionic dynamics, approximation free, vibration suppression, active suspension.**

Manuscript received 24 July 2023; accepted 17 August 2023. Date of publication 11 September 2023; date of current version 16 October 2024. This article was recommended for publication by Associate Editor G. Chen and Editor D. Song upon evaluation of the reviewers' comments. This work was supported in part by the National Natural Science Foundation of China under Grant 62173108 and Grant 62022031, in part by the Postdoctoral Science Foundation of Heilongjiang under Grant LBH-TZ2111, and in part by the Fundamental Research Funds for the Central Universities under Grant HIT.OCEF.2022012. *(Corresponding author: Huihui Pan.)*

Tenglong Huang and Huihui Pan are with the Research Institute of Intelligent Control and Systems, Harbin Institute of Technology, Harbin 150001, China (e-mail: huangtenglong@hit.edu.cn; huihuipan@hit.edu.cn).

Jue Wang is with the Ningbo Institute of Intelligent Equipment Technology Company Ltd., Ningbo 315200, China, and also with the Department of Automation, University of Science and Technology of China, Hefei 230027, China (e-mail: juewang@hit.edu.cn).

Color versions of one or more figures in this article are available at https://doi.org/10.1109/TASE.2023.3310335.

Digital Object Identifier 10.1109/TASE.2023.3310335

I. Introduction

VEHICLE vibration [1], [2], [3], [4] is inevitable when the vehicle is driving on an uneven road, which can deteriorate vehicle performance. Suppressing vehicle vibrations helps to improve ride comfort and safety, while reducing the adverse effects of vibration, including damage to components and reduced vehicle lifetime. Vehicle suspension control [5], [6], [7] provides an effective solution to suppress vehicle vibration and thus attracts a great deal of interest from automotive engineers and scientists. By devising suspension controllers, it is desired that the external perturbations and system uncertainties, including parameter uncertainties and model uncertainties, can be handled efficiently to achieve fast vibrations isolation while enhancing the reliability against faults and reducing energy consumption.

Suspension controllers are mainly applied for active and semi-active suspensions (SAS) [5]. Compared with SAS, active suspension (AS) [6] has a higher control degree of freedom and thus is more flexible. However, the energy consumption of AS [7] is generally higher than SAS. To reduce energy consumption, a self-powered suspension with special circuits is designed in [8] to regenerate and save energy. Such special circuits in [8] can be effective in reducing energy consumption but require changes in the hardware structure of AS, which makes it difficult and expensive to deploy and limits the application of this approach. The MPC approach proposed in [9] introduces energy consumption into the cost function to achieve energy savings by optimization. In [10], game theory is used to develop specific rules to balance ride comfort and energy consumption. In particular, an interesting X-type bionic suspension inspired by animal limb structures contributes to reducing energy consumption, as analyzed in [11]. Compared with embedding self-powered circuits into AS [8] or optimizing special cost functions, introducing bionic dynamics [12], [13] is more convenient to deploy in practice. For this reason, this paper focuses on designing a bionic

1545-5955 © 2023 IEEE. Personal use is permitted, but republication/redistribution requires IEEE permission.
See https://www.ieee.org/publications/rights/index.html for more information.

Authorized licensed use limited to: GUANGZHOU UNIVERSITY. Downloaded on November 21,2024 at 07:08:04 UTC from IEEE Xplore. Restrictions apply.

energy-saving control scheme for AS to achieve flexible and efficient vibration suppression.

Numerous control methods are employed to develop suspension controllers [14]. The adaptive backstepping-based controller in [7] allows the system error signals and states to be bounded. Employing the linear matrix inequality, the H_∞ controller proposed in [15] achieves asymptotic stability of the closed-loop system, namely, the state signals tend to 0 as $t \to \infty$. The error signals can converge to a neighborhood of 0 in finite time using the presented sliding mode controller in [16]. However, the finite convergence time depends on the initial value and the controller parameters. The fixed time controller [17] can remove the dependence on the initial value. However, it is still limited by the controller parameters and the first-order derivatives of perturbations are assumed to be bounded. Prespecified time control [18] methods can explicitly specify the settling time, which is completely independent of the controller parameters and the initial value. The novel prescribed time controller in [19] theoretically guarantees the error signals converge to 0 over finite time intervals. However, it may be unrealistic in practice as the noise will be amplified at the prespecified settling time instant [20]. It is more reasonable to make the error signals or states converge to a neighborhood of 0 at the prespecified time for practical applications [18].

In addition, the following difficulties are common in real systems, which need to be considered to guarantee or enhance controller performance.

- *Uncertainties:* The model-based controllers [7] require the prior models and parameters information and the performance is closely associated with the information accuracy. However, collecting accurate system information is unrealistic. Neural networks [21] or fuzzy rules can be employed to approximate the unknown model, nonetheless, which introduces new challenges, including designing network structure, training data collection, constructing fuzzy rule bases, etc.
- *Disturbances:* To further enhance the robustness, the external disturbances can be handled using embedded structures such as disturbance observer and adaptive estimation [8]. Correspondingly, it leads to high controller complexity or requires stringent assumptions for example bounded first-order derivatives.
- *Faults:* Actuators faults [22], [23], [24] caused by aging and wear, etc, can affect system performance adversely. Seeking a solution to address the occurred faults is a hot topic. By introducing fault detection and estimation mechanisms, some existing results can achieve effective fault-tolerant control.

However, constructing neural network structures, designing enough fuzzy rules, and developing disturbance observers or fault estimators are inherently challenging. Meanwhile, the mentioned approach increase controller complexity and the difficulty of the controller design and application. In contrast, time delay estimation (TDE) [24] allows the control scheme to be independent of the model knowledge and does not require additional complex mechanisms. Consequently, the controller complexity can be reduced and a simple and efficient controller is possible.

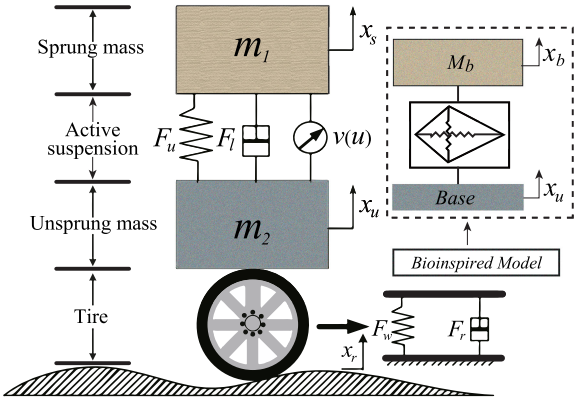

Fig. 1. Schematic of a quarter-vehicle active suspension.

Motivated by the analysis above, this paper presents an approximation-free energy-efficient prespecified-time reliable control framework utilizing bionic dynamics and time-delay information. The main contributions are listed as follows:

1) A prespecified time controller is designed that can make the steady-state responses of error signals converge to a neighborhood of 0 over a prespecified finite time interval. Meanwhile, the system transient responses satisfy the performance constraints. Compared with the conventional asymptotically stability, finite-time stability [25], and fixed-time stability, the prespecified convergence time is completely independent of the initial values and controller parameters [18].
2) By introducing time delay information, the designed control scheme is model-free and approximation-free. Namely, the model knowledge and approximation structures, such as neural networks or fuzzy logic [26], are unnecessary. Meanwhile, the proposed controller is robust to unknown external disturbances. Actuator faults, including loss-of-effectiveness faults and bias faults, can be effectively compensated and handled to enhance reliability.
3) Inspired by animal bionic structures [11], asymmetric X-type bio-inspired dynamics are embedded into this controller, which further reduces energy consumption. The proposed energy-efficient control framework does not need to solve optimization problems, nor change the hardware structure with the regenerative circuits [8]. Simple and effective energy-efficient control with reliable vibration isolation is achieved.

II. Problem Formulation

The detailed structure of the quarter-vehicle active suspension is illustrated in Fig. 1. The vehicle body mass is denoted as the sprung mass m_1, and the unsprung mass m_2 represents the wheel mass. The damping and elastic forces of active suspension are represented as F_l and F_u. Correspondingly, F_w and F_r are the elastic force and damping force of the tire under the road excitation x_r, respectively. $\dot{x}_s$ and $\dot{x}_u$ are the sprung and unsprung mass velocities,

Authorized licensed use limited to: GUANGZHOU UNIVERSITY. Downloaded on November 21,2024 at 07:08:04 UTC from IEEE Xplore. Restrictions apply.

and the corresponding displacements are denoted as x_s and x_u, respectively. Define $\xi_1{:=}x_s$, $\xi_2{:=}\dot{x}_s$, $\xi_3{:=}x_u$, $\xi_4{:=}\dot{x}_u$, the nonlinear suspension model [16] can be formulated as follows:

$$\dot{\xi}_1 = \xi_2 \tag{1}$$

$$\dot{\xi}_2 = \frac{1}{m_1}(-F_l(\dot{x}_s, \dot{x}_u, t) - F_u(x_s, x_u, t) + v(u(t))) + d_1 \tag{2}$$

$$\dot{\xi}_3 = \xi_4 \tag{3}$$

$$\dot{\xi}_4 = \frac{1}{m_2}(F_l(\dot{x}_s, \dot{x}_u, t) + F_u(x_s, x_u, t) - F_w(x_u, x_r, t) - F_r(\dot{x}_u, \dot{x}_r, t) - v(u(t))) + d_2 \tag{4}$$

$$y = \xi_1 \tag{5}$$

with

$$F_u(x_s, x_u, t) = p_{s1}(x_s - x_u) + p_{s2}(x_s - x_u)^3,$$
$$F_l(\dot{x}_s, \dot{x}_u, t) = k_{lp}(\dot{x}_s - \dot{x}_u),\ k_{lp} = \begin{cases} k_l, (\dot{x}_s - \dot{x}_u) > 0 \\ k_p, (\dot{x}_s - \dot{x}_u) \le 0 \end{cases}$$
$$F_w(x_u, x_r, t) = p_w(x_u - x_r),\ F_r(\dot{x}_u, \dot{x}_r, t) = k_r(\dot{x}_u - \dot{x}_r)$$

where p_{s1}, p_{s2}, k_l and k_p are the suspension linear, nonlinear stiffness, and damping coefficients. $v(u(t))$ is the actual signal of the actuator and $u(t)$ denotes the control input to be designed. The tire stiffness and damping coefficients are denoted as p_w and k_r. d_1 and d_2 are the unknown external unmatched disturbance.

Inspired by animal skeleton structure, it is possible to enhance the energy efficiency of the active suspension system with the help of bionic dynamics by exploiting the beneficial nonlinear properties. As depicted on the right side of Fig. 1, bionic dynamics is introduced as a reference model to improve energy-saving characteristics in this paper. In addition to vibration suppression and low energy consumption, reliability is also crucial for vehicle suspension. Specifically, the following actuator faults [24], [27] are considered and addressed in this paper, modeled as

$$v(u(t)) = \zeta(t)u(t) + \zeta_b(t) \tag{6}$$

where $0 < \zeta(t) \le 1$ is the unknown time-varying loss-of-effectiveness (LOE) coefficient of actuator. $\zeta_b(t) \ge 0$ represents the unknown time-varying actuator bias fault (BF). Note that the following cases are covered in (6): 1) $\zeta(t) = 1$, $\zeta_b(t) = 0$, fault-free case; 2) $\zeta(t) = 1$, $\zeta_b(t) \ne 0$ indicates that lock-in-place (LIP) fault exists; 3) $\zeta(t) \in (0, 1)$, $\zeta_b(t) = 0$ means that LOE fault exists; 4) $\zeta(t) \in (0, 1)$, $\zeta_b(t) \ne 0$ indicates both LOE and BF faults exist.

The suspension sprung system model with actuator faults can be reformulated as

$$\dot{\xi}_1 = \xi_2 \tag{7}$$

$$\dot{\xi}_2 = f(\xi_1,\xi_2, t) + g(\xi_1,\xi_2, t)u + h(\xi_1,\xi_2, t) \tag{8}$$

$$y = \xi_1 \tag{9}$$

where $f(\xi_1,\xi_2, t) = \frac{1}{m_1}(-F_l(\dot{x}_s, \dot{x}_u, t) - F_u(x_s, x_u, t))$, $g(\xi_1,\xi_2, t) = \frac{\zeta(t)}{m_1}$, $h(\xi_1,\xi_2, t) = \frac{\zeta_b(t)}{m_1} + d_1$.

Specifically, the following aspects are taken into account for the controller design in this paper:

- Ride comfort; superior ride comfort means that the vehicle vibration is suppressed quickly and effectively. Vertical acceleration is used as the performance indicator of ride comfort for quantitative assessment.
- Low energy consumption; introducing beneficial nonlinearities by combing animal limb dynamics to further reduce energy consumption.
- Reliability; actuator faults [28], caused by mechanical mechanism wear, aging, etc, are handled to enhance the reliability of the suspension system.
- Robustness; model uncertainties, parameter uncertainties, and unknown external perturbations are also taken into consideration.

In general, this paper focuses on an energy-efficient approximation-free controller design with fast pre-assigned time convergence properties, which can suppress the vibration effectively while handling unknown time-varying actuator failures, model uncertainty, parameter uncertainty, and external disturbance with low energy consumption.

Definition 1: The system $\dot{\varkappa} = f(\varkappa, t), \varkappa \in \mathbb{R}^n$ is said to achieve practical prespecified time (PST) convergence [18], [19], [29], [30] if there exists a settling time T_s and a constant ϱ such that

$$\|\varkappa\| < \varrho, \text{ for } t > T_s, \forall \varkappa(0) = \varkappa_0 \tag{10}$$

where $T_s > 0$, and $\varrho \in \mathbb{R}^+$ are the parameters selected by the user. The settling time T_s is completely independent of the initial conditions $\varkappa_0$ and controller parameters.

Assumption 1: The actuator bias fault $\zeta_b(t)$ and external disturbance d_i are bounded, namely

$$|\zeta_b(t)| \le \bar{\zeta}_b,\ |d_i| \le \bar{d}_i, i = 1, 2 \tag{11}$$

where $\bar{\zeta}_b$, $\bar{d}_i$ are unknown positive constants. Recall that (9), $h(\xi_1,\xi_2, t) \le \bar{h}$ holds. $\bar{h} = \frac{\bar{\zeta}_b}{m_1} + \bar{d}_1$ is a unknown positive constant.

III. Main Results

In this section, detailed descriptions of the introduced time-delay estimation technique are given first. Aiming to reduce energy consumption, based on bionic structural properties analysis [11], bionic dynamics are designed to provide a reference trajectory for the active suspension. Then, the approximation-free prespecified time controller is developed by employing function transformation and time delay information, while the detailed theoretical proof of the devised control framework is presented.

A. Time Delay Estimation

The sprung suspension system with actuator failures (5)-(9) can be reformulated as

$$\dot{\xi}_1 = \xi_2 \tag{12}$$

$$\dot{\xi}_2 = \Xi(\xi_1,\xi_2, t) + \bar{\mathcal{S}}^{-1}u \tag{13}$$

$$y = \xi_1 \tag{14}$$

where

$$\Xi(\xi_1,\xi_2, t) = f(\xi_1,\xi_2, t) + g(\xi_1,\xi_2, t)u - \bar{\mathcal{S}}^{-1}u + h(\xi_1,\xi_2, t) \tag{15}$$

Authorized licensed use limited to: GUANGZHOU UNIVERSITY. Downloaded on November 21,2024 at 07:08:04 UTC from IEEE Xplore. Restrictions apply.

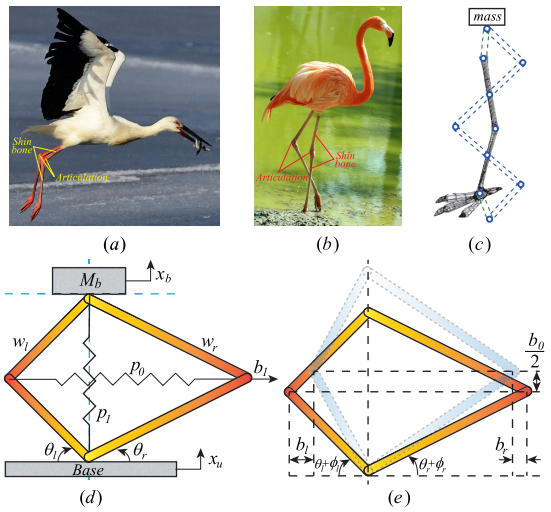

Fig. 2. Asymmetrical X-shaped bionic limb structures present in animals.

and $\bar{\mathcal{S}} \in \mathbb{R}^+$ is a introduced constant. The nonlinear function $\Xi(\xi_1,\xi_2,t)$ can be estimated by employing the time delay information, and the detailed analysis of TDE can be found in [31]. The effectiveness of the TDE has been verified in vehicle-integrated motion control [24], robot manipulators, and six-phase induction motor [31]. Using the time delay information, when $\mathcal{T}$ is small enough, we can obtain

$$\Xi(\xi_1,\xi_2,t) \approx \hat{\Xi}(\xi_1,\xi_2,t) = \Xi(\xi_1,\xi_2,t-\mathcal{T}) \tag{16}$$

where $\hat{\Xi}(\xi_1,\xi_2,t)$ is the estimation of $\Xi(\xi_1,\xi_2,t)$. Correspondingly, the time delay estimation error σ can be calculated as

$$\sigma = \Xi(\xi_1,\xi_2,t) - \hat{\Xi}(\xi_1,\xi_2,t) \tag{17}$$

The boundedness of σ will be given later.

By introducing the time delay information (16), the suspension sprung system (7)-(9) with actuator faults (6) can be rewritten as

$$\dot{\xi}_1 = \xi_2 \tag{18}$$

$$\dot{\xi}_2 = \Xi(\xi_1,\xi_2,t-\mathcal{T}) + \bar{\mathcal{S}}^{-1}u + \sigma \tag{19}$$

$$y = \xi_1 \tag{20}$$

where, $\Xi(\xi_1,\xi_2,t-\mathcal{T})$ can be obtained from (12)-(17) by

$$\Xi(\xi_1,\xi_2,t-\mathcal{T}) = \dot{\xi}_2(t-\mathcal{T}) - \bar{\mathcal{S}}^{-1}u(t-\mathcal{T}) \tag{21}$$

B. Bionic Reference Dynamics

Aiming to achieve energy-saving properties, bionic structures are introduced and analyzed in this section. Asymmetric X-shaped structures are naturally present in animal limbs, such as the white stork in Fig. 2(a) and the flamingo in Fig. 2(b). Fig. 2(c) highlights and illustrates the presence of X-shaped structures. Inspired by the animal limbs, the static bionic dynamical structure is modeled as in Fig. 2(d). The lengths of the left and right rods of the bionic structure are w_l and w_r, and the corresponding static angles with the base are θ_l and θ_r, respectively. The equivalent lateral and vertical spring stiffnesses are p_0 and p_1. The structure deformation under external excitation is illustrated in Fig. 2(e). ϕ_l and ϕ_r represent the left and right angular deformations, and the corresponding displacements are b_l and b_r. b_0 denotes the vertical relative displacement of M_b with respect to the base, namely, $b_0 = x_b - x_u$. According to the geometric relationship in Fig. 2(d) and (e), we can obtain

$$\phi_k = \arctan\left(\frac{w_k \sin\theta_k + \frac{b_0}{2}}{w_k\cos\theta_k - b_k}\right) - \theta_k \tag{22}$$

$$b_k = w_k\cos\theta_k - \sqrt{w_k^2 - \left(w_k\sin\theta_k + \frac{b_0}{2}\right)^2} \tag{23}$$

where $k = l, r$. Define $\phi := \phi_l + \phi_r$, $b_1 := b_l + b_r$, and

$$g_1(b_0) := p_0 b_1 \frac{d(b_1)}{d(b_0)}\frac{d(b_0)}{d(x_b)},\ g_2(b_0) := \left(\frac{d\phi}{d(b_0)}\right)^2 \tag{24}$$

By employing the Lagrange principle [11], the X-shaped bionic reference dynamics can be expressed as

$$M_b\ddot{b}_0 + M_b\ddot{x}_u = -g_1(b_0) - p_1 b_0 - \lambda_1\dot{b}_0 - \lambda_2 q_n g_2(b_0)\dot{b}_0 \tag{25}$$

where λ_1 and λ_2 denote the air drag and the rotation friction factors. $g_1(b_0)$ and $g_2(b_0)$ in (24) can be calculated by

$$g_1(b_0) = \frac{p_0}{2}\left(w_l\cos\theta_l + w_r\cos\theta_r - \sqrt{w_l^2 - \Upsilon^2(b_0)} - \sqrt{w_r^2 - \Upsilon^2(b_0)}\right) \times \left(\frac{\Upsilon(b_0)}{\sqrt{w_l^2 - \Upsilon^2(b_0)}} + \frac{\Upsilon(b_0)}{\sqrt{w_r^2 - \Upsilon^2(b_0)}}\right) \tag{26}$$

$$g_2(b_0) = \left(\frac{1}{2\sqrt{w_l^2 - \Upsilon^2(b_0)}} + \frac{1}{2\sqrt{w_r^2 - \Upsilon^2(b_0)}}\right)^2 \tag{27}$$

where $\Upsilon(b_0) := w_l\sin\theta_l + \frac{b_0}{2}$.

Introducing the animal limb-inspired asymmetric X-shaped structure [12] to employ the beneficial nonlinearities present in the structure, can help to reduce energy consumption while suppressing vehicle vibration and improving ride comfort [13]. In practice, the detailed structural characterization analysis in [11] can be used to rationally select the X-type structural parameters. More detailed information about the advantages and characteristics of bionic dynamics in engineering applications can be found in [12].

C. Approximation-Free Global Prespecified Time Controller Design

The details of the developed practical prespecified time controller based on time delay information to achieve effective vibration suppression with low energy consumption are elaborated in this section. The vibration suppression problem for the suspension sprung system (7)-(9) is converted into a reference dynamics (25) tracking problem. Meanwhile, the robustness to external disturbances, parameter uncertainties, model uncertainties, and reliability against actuator faults are enhanced by the proposed controller. Specifically, the tracking error variable e_1 is defined as

$$e_1 = y - y_r = \xi_1 - \xi_{1r} \tag{28}$$

Authorized licensed use limited to: GUANGZHOU UNIVERSITY. Downloaded on November 21,2024 at 07:08:04 UTC from IEEE Xplore. Restrictions apply.

where the reference signal y_r can be obtained from the bionic dynamics (25). The following special error constraint function $\mathcal{Q}(t)$ is introduced into the presented control scheme:

$$\mathcal{Q}(t) = \begin{cases} \left(\frac{1}{t} - \frac{1}{T_\zeta}\right)^{2\mathcal{L}} + \mathcal{Q}_\varrho, & 0 \le t \le T_\zeta \\ \mathcal{Q}_\varrho, & t > T_\zeta \end{cases} \tag{29}$$

where $\mathcal{L}$ is a positive integer and subject to $\mathcal{L} \ge 2$. T_ζ is the prespecified setting time and $\mathcal{Q}_\varrho$ is the prescribed steady-state error constraint. $\mathcal{Q}(t)$ to be infinite at the initial instant allows it to obtain a global result. For simplicity, we define $\mathcal{Q}(t)$, whose first-order derivative $\dot{\mathcal{Q}}(t)$, and second-order derivative $\ddot{\mathcal{Q}}(t)$ are equal to $+\infty$ at the initial instant in this paper, namely, $\mathcal{Q}(0)=\dot{\mathcal{Q}}(0)=\ddot{\mathcal{Q}}(0)=+\infty$. $\mathcal{Q}_\varrho$ and T_ζ can be tuned and specified by the user, as required.

Based on the error constraint function (29), the following error transformation is introduced

$$\eta_1(t) := \frac{e_1(t)}{\mathcal{F}(\mathcal{D}(t))} \tag{30}$$

where $\mathcal{D}(t)$ denotes the distance of the transformed error signal from the error constraint $\mathcal{Q}(t)$. The real-time distance $\mathcal{D}(t)$ at the time instant t with $\kappa \in \mathbb{R}^+$ can be calculated by

$$\begin{aligned} \mathcal{D}(t) &= \kappa(e_1(t) - (-\mathcal{Q}(t)))(\mathcal{Q}(t) - e_1(t)) \\ &= \kappa\mathcal{Q}^2(t) - \kappa e_1^2(t) \end{aligned} \tag{31}$$

Combined with the distance function $\mathcal{D}(t)$ defined in (31), the transformation function $\mathcal{F}(\mathcal{D}(t))$ in (30) can be written in the form

$$\mathcal{F}(\mathcal{D}(t)) = \begin{cases} 1 - \left(\frac{\mathcal{D}(t)}{\mathcal{R}_s} - 1\right)^{2\mathcal{L}}, & 0 < \mathcal{D}(t) \le \mathcal{R}_s \\ 1, & \mathcal{D}(t) > \mathcal{R}_s \end{cases} \tag{32}$$

where $\mathcal{R}_s \in \mathbb{R}^+$. The error variable $e_1(t)$ is taken to be within the safe region when $\mathcal{D}(t) \in (0, \mathcal{R}_s]$.

In conjunction with the error transformation (30) and time delay information (20) and (21) introduced above, the virtual and actual control laws of the proposed approximation-free prespecified time control framework are designed in two steps. In *Step 1*, the candidate Lyapunov function is selected as

$$V_1 = \frac{1}{2}\eta_1^2 \tag{33}$$

Then, we can obtain $\dot{V}_1 = \eta_1\dot{\eta}_1$. The derivative of the transformed error variable η_1 in (30) can be derived from (18)-(19), which is given by

$$\begin{aligned} \dot{\eta}_1 &= \chi_1\dot{e}_1 + \psi_1 \\ &= \chi_1(\xi_2 - \dot{y}_r) + \psi_1 \end{aligned} \tag{34}$$

where χ_1 and ψ_1 are defined as

$$\chi_1 = \begin{cases} -\frac{4\kappa\mathcal{L}}{\mathcal{R}_s\mathcal{F}^2}\left(\frac{\mathcal{D}(t)}{\mathcal{R}_s} - 1\right)^{2\mathcal{L}-1} e_1^2 + \frac{1}{\mathcal{F}}, & 0 < \mathcal{Q}(t) \le \mathcal{R}_s \\ 1, & \mathcal{Q}(t) > \mathcal{R}_s \end{cases} \tag{35}$$

$$\psi_1 = \begin{cases} \frac{4\kappa\mathcal{L}}{\mathcal{R}_s\mathcal{F}^2}\left(\frac{\mathcal{D}(t)}{\mathcal{R}_s} - 1\right)^{2\mathcal{L}-1} \mathcal{Q}\dot{\mathcal{Q}}e_1, & 0 < \mathcal{Q}(t) \le \mathcal{R}_s \\ 0, & \mathcal{Q}(t) > \mathcal{R}_s \end{cases} \tag{36}$$

$$\dot{\mathcal{Q}}(t) = \begin{cases} 2\mathcal{L}\left(\frac{1}{t} - \frac{1}{T_\zeta}\right)^{2\mathcal{L}-1} \frac{-1}{t^2}, & 0 \le t \le T_\zeta \\ 0, & t > T_\zeta \end{cases} \tag{37}$$

Meanwhile, the following change of the coordinate is introduced

$$\eta_2 := \xi_2 - \alpha_1 \tag{38}$$

where α_1 denotes the virtual control law. The error variable η_1 dynamic in (34) can be rewritten as

$$\dot{\eta}_1 = \chi_1(\eta_2 + \alpha_1 - \dot{y}_r) + \psi_1 \tag{39}$$

Then, we get

$$\dot{V}_1 = \chi_1(\eta_1\eta_2 + \eta_1\alpha_1 - \eta_1\dot{y}_r) + \eta_1\psi_1 \tag{40}$$

The virtual control input α_1 is chosen as follow

$$\alpha_1 = -\frac{\rho_1}{\chi_1}\eta_1 - \chi_1\dot{y}_r^2\eta_1 - \frac{\psi_1^2}{\chi_1}\eta_1 \tag{41}$$

where ρ_1 is a positive real number.

In *Step 2*, combining the coordinate change in (38) and the suspension system (20) with time delay information in (21), the dynamic of η_2 can be calculated as

$$\begin{aligned} \dot{\eta}_2 &= \dot{\xi}_2 - \dot{\alpha}_1 \\ &= \Xi(\xi_1, \xi_2, t - \mathcal{T}) + \bar{\mathcal{S}}^{-1}u + \sigma - \dot{\alpha}_1 \end{aligned} \tag{42}$$

It can be observed from (41) that α_1 is a function with respect to ξ_1, y_r, $\dot{y}_r$, $\mathcal{Q}$, and $\dot{\mathcal{Q}}$. Therefore, it follows that

$$\dot{\alpha}_1 = \frac{\partial\alpha_1}{\partial\xi_1}\xi_2 + \frac{\partial\alpha_1}{\partial\mathcal{Q}}\dot{\mathcal{Q}} + \frac{\partial\alpha_1}{\partial\dot{\mathcal{Q}}}\ddot{\mathcal{Q}} + \frac{\partial\alpha_1}{\partial y_r}\dot{y}_r + \frac{\partial\alpha_1}{\partial\dot{y}_r}\ddot{y}_r \tag{43}$$

with

$$\ddot{\mathcal{Q}}(t) = \begin{cases} 2\mathcal{L}\Big((2\mathcal{L}-1)\left(\frac{1}{t} - \frac{1}{T_\zeta}\right)^{2\mathcal{L}-2} t^{-4} \\ \quad + \left(\frac{1}{t} - \frac{1}{T_\zeta}\right)^{2\mathcal{L}-1} 2t^{-3}\Big), & 0 \le t \le T_\zeta \\ 0, & t > T_\zeta \end{cases} \tag{44}$$

The designed actual control input u in *Step 2* is provided as follows

$$\begin{aligned} u = \bar{\mathcal{S}}\Big(&-\rho_2\eta_2 - \hat{\Xi}(\xi_1, \xi_2, t) - \chi_1^2\eta_1\eta_2 - \frac{1}{\iota_3}\chi_1^2\eta_1^2\eta_2^2 - \frac{\eta_2}{\gamma} \\ &- \frac{\eta_2}{\beta_1}\left(\frac{\partial\alpha_1}{\partial\xi_1}\xi_2\right)^2 - \frac{\eta_2}{\beta_2}\left(\frac{\partial\alpha_1}{\partial\mathcal{Q}}\dot{\mathcal{Q}}\right)^2 - \frac{\eta_2}{\beta_3}\left(\frac{\partial\alpha_1}{\partial\dot{\mathcal{Q}}}\ddot{\mathcal{Q}}\right)^2 \\ &- \frac{\eta_2}{\beta_4}\left(\frac{\partial\alpha_1}{\partial y_r}\dot{y}_r\right)^2 - \frac{\eta_2}{\beta_5}\left(\frac{\partial\alpha_1}{\partial\dot{y}_r}\ddot{y}_r\right)^2\Big) \end{aligned} \tag{45}$$

where $\rho_2 \in \mathbb{R}^+$. ι_3, γ, and β_i, $i = 1, 2, 3, 4, 5$ are the controller parameters, which are positive real numbers and defined below. The time delay estimation $\hat{\Xi}(\xi_1, \xi_2, t)$ can be computed from (14)-(21). As formulated in (5)-(9), $f(\xi_1, \xi_2, t)$ only contains the elastic force F_u and damping force F_l of the suspension. The nonlinear term $f(\xi_1, \xi_2, t)$ in $\Xi(\xi_1, \xi_2, t)$ is continuous. In conjunction with (6) and Assumption 1, it can be concluded that $g(\xi_1, \xi_2, t)$ and $h(\xi_1, \xi_2, t)$ are bounded. Meanwhile, the designed controller u is continuous. As detailed in [31], the upper bound of the time delay estimation error σ exists in this case, namely,

$$|\sigma| \le \sigma_B \tag{46}$$

Authorized licensed use limited to: GUANGZHOU UNIVERSITY. Downloaded on November 21,2024 at 07:08:04 UTC from IEEE Xplore. Restrictions apply.

where $\sigma_B \in \mathbb{R}^+$ is an unknown constant, which is unnecessary for the controller design. As in (41) and (45), the developed controller u and virtual control input α_1 are completely independent of the actuator fault information and model information of the suspension system (5).

With the proposed control inputs α_1 and u, the following theorem hold.

Theorem 1: For vehicle active suspension system (7)-(9) with actuator faults (6), the practical prespecified time stabilization (10) of the suspension system can be achieved by employing the proposed approximation-free virtual control input α_1 in (41) and the fault-tolerant controller u in (45). In specific,

a) The bionic reference dynamic tracking error e_1 satisfies

$$\|e_1\| < \mathcal{R}_s, \text{ for } \forall e_1(0) \in \mathbb{R} \text{ and } t > T_\zeta \tag{47}$$

where $T_\zeta \in \mathbb{R}^+$ is the prespecified settling time, and $\mathcal{R}_s \in \mathbb{R}^+$ is the steady-state tracking error constraint. The convergence time T_ζ and the steady-state performance constraint $\mathcal{R}_s$ are completely independent of controller parameters and the initial condition of the suspension system.

b) The closed-loop system is stable and all signals are bounded.

D. Stability Analysis

The stability of the closed-loop system with prespecified time convergence property, as detailed in *Theorem 1*, is analyzed and proved in this section. The transformed error variable η_1 is bounded by using the time delay estimation-based approximation-free control scheme in (41) and (45). Accordingly, the prespecified time convergence property of the reference dynamics tracking error e_1 is guaranteed.

Recall that the derivative of the Lyapunov function V_1 in *Step 1*, combining the designed virtual control law (41) and (40), we get

$$\dot{V}_1 = \chi_1\eta_1\alpha_1 + \chi_1\eta_1\eta_2 - \chi_1\eta_1\dot{y}_r + \eta_1\psi_1 \tag{48}$$

Substituting the virtual control law (41) into $\chi_1\eta_1\alpha_1$, yields

$$\begin{aligned}\chi_1\eta_1\alpha_1 &= \chi_1\eta_1\left(-\frac{\rho_1}{\chi_1}\eta_1 - \chi_1\dot{y}_r^2\eta_1 - \frac{\psi_1^2}{\chi_1}\eta_1\right)\\ &= -\rho_1\eta_1^2 - \chi_1^2\dot{y}_r^2\eta_1^2 - \psi_1^2\eta_1^2\end{aligned} \tag{49}$$

Thus, we can obtain

$$\begin{aligned}\dot{V}_1 = &-\rho_1\eta_1^2 + \eta_1\psi_1 - \chi_1^2\dot{y}_r^2\eta_1^2 - \psi_1^2\eta_1^2\\ &- \chi_1\eta_1\dot{y}_r + \chi_1\eta_1\eta_2\end{aligned} \tag{50}$$

By applying Young's inequality, the following inequalities hold

$$\eta_1\psi_1 \le \frac{1}{\iota_1}\eta_1^2\psi_1^2 + \frac{\iota_1}{4} \tag{51}$$

$$-\chi_1\eta_1\dot{y}_r \le \frac{1}{\iota_2}\chi_1^2\dot{y}_r^2\eta_1^2 + \frac{\iota_2}{4} \tag{52}$$

$$\chi_1\eta_1\eta_2 \le \frac{1}{\iota_3}\chi_1^2\eta_1^2\eta_2^2 + \frac{\iota_3}{4} \tag{53}$$

where ι_1, ι_2, and ι_3 are positive real numbers. Summing (49) and the inequalities (51)-(53), we can get

$$\begin{aligned}\dot{V}_1 &\le -\rho_1\eta_1^2 - \chi_1^2\dot{y}_r^2\eta_1^2 - \psi_1^2\eta_1^2 + \frac{1}{\iota_1}\eta_1^2\psi_1^2\\ &\quad + \frac{\iota_1}{4} + \frac{1}{\iota_2}\chi_1^2\dot{y}_r^2\eta_1^2 + \frac{\iota_2}{4} + \frac{1}{\iota_3}\chi_1^2\eta_1^2\eta_2^2 + \frac{\iota_3}{4}\\ &\le -\rho_1\eta_1^2 + \frac{1}{\iota_3}\chi_1^2\eta_1^2\eta_2^2 + \frac{\sum_{i=1}^3\iota_i}{4}\end{aligned} \tag{54}$$

The candidate Lyapunov function V_2 is defined as follows

$$V_2 = \frac{1}{2}\eta_2^2 \tag{55}$$

Invoking the derivative of the η_2 in (42), the dynamic of V_2 can be expressed as

$$\begin{aligned}\dot{V}_2 &= \eta_2\dot{\eta}_2\\ &= \eta_2\hat{\Xi}(\xi_1,\xi_2,t) + \eta_2\bar{\mathcal{S}}^{-1}u + \eta_2\sigma - \eta_2\dot{\alpha}_1\end{aligned} \tag{56}$$

According to Young's inequality and the analysis (46) of the time-delay estimation, we have

$$\eta_2\sigma \le \frac{1}{\gamma}\eta_2^2 + \frac{\gamma\sigma_B^2}{4}$$

where $\gamma > 0$. Meanwhile, combining the dynamic of virtual control law α_1 in (43) and Young's inequality, we can obtain

$$\begin{aligned}-\eta_2\dot{\alpha}_1 &\le |\eta_2|\left|\frac{\partial\alpha_1}{\partial\xi_1}\xi_2 + \frac{\partial\alpha_1}{\partial\mathcal{Q}}\dot{\mathcal{Q}} + \frac{\partial\alpha_1}{\partial\dot{\mathcal{Q}}}\ddot{\mathcal{Q}} + \frac{\partial\alpha_1}{\partial y_r}\dot{y}_r + \frac{\partial\alpha_1}{\partial\dot{y}_r}\ddot{y}_r\right|\\ &\le \frac{1}{\beta_1}\eta_2^2\left(\frac{\partial\alpha_1}{\partial\xi_1}\xi_2\right)^2 + \frac{\beta_1}{4} + \frac{1}{\beta_2}\eta_2^2\left(\frac{\partial\alpha_1}{\partial\mathcal{Q}}\dot{\mathcal{Q}}\right)^2 + \frac{\beta_2}{4}\\ &\quad + \frac{1}{\beta_3}\eta_2^2\left(\frac{\partial\alpha_1}{\partial\dot{\mathcal{Q}}}\ddot{\mathcal{Q}}\right)^2 + \frac{\beta_3}{4} + \frac{1}{\beta_4}\eta_2^2\left(\frac{\partial\alpha_1}{\partial y_r}\dot{y}_r\right)^2\\ &\quad + \frac{\beta_4}{4} + \frac{1}{\beta_5}\eta_2^2\left(\frac{\partial\alpha_1}{\partial\dot{y}_r}\ddot{y}_r\right)^2 + \frac{\beta_5}{4}\\ &\le \eta_2^2\left(\frac{1}{\beta_1}\left(\frac{\partial\alpha_1}{\partial\xi_1}\xi_2\right)^2 + \frac{1}{\beta_2}\left(\frac{\partial\alpha_1}{\partial\mathcal{Q}}\dot{\mathcal{Q}}\right)^2\right.\\ &\quad + \frac{1}{\beta_3}\left(\frac{\partial\alpha_1}{\partial\dot{\mathcal{Q}}}\ddot{\mathcal{Q}}\right)^2 + \frac{1}{\beta_4}\left(\frac{\partial\alpha_1}{\partial y_r}\dot{y}_r\right)^2 + \frac{\sum_{i=1}^5\beta_i}{4}\\ &\quad \left.+ \frac{1}{\beta_5}\left(\frac{\partial\alpha_1}{\partial\dot{y}_r}\ddot{y}_r\right)^2\right)\end{aligned} \tag{57}$$

where $\beta_i \in \mathbb{R}^+$, $i = 1, 2, 3, 4, 5$. Thus,

$$\begin{aligned}\eta_2\sigma - \eta_2\dot{\alpha}_1 &\le \eta_2^2\left(\frac{1}{\beta_1}\left(\frac{\partial\alpha_1}{\partial\xi_1}\xi_2\right)^2 + \frac{1}{\beta_2}\left(\frac{\partial\alpha_1}{\partial\mathcal{Q}}\dot{\mathcal{Q}}\right)^2\right.\\ &\quad + \frac{1}{\beta_3}\left(\frac{\partial\alpha_1}{\partial\dot{\mathcal{Q}}}\ddot{\mathcal{Q}}\right)^2 + \frac{1}{\beta_4}\left(\frac{\partial\alpha_1}{\partial y_r}\dot{y}_r\right)^2\\ &\quad \left.+ \frac{1}{\beta_5}\left(\frac{\partial\alpha_1}{\partial\dot{y}_r}\ddot{y}_r\right)^2\right) + \frac{1}{\gamma}\eta_2^2 + \frac{\gamma\sigma_B^2}{4} + \frac{\sum_{i=1}^5\beta_i}{4}\\ &\le \eta_2^2\left(\frac{1}{\beta_1}\left(\frac{\partial\alpha_1}{\partial\xi_1}\xi_2\right)^2 + \frac{1}{\beta_2}\left(\frac{\partial\alpha_1}{\partial\mathcal{Q}}\dot{\mathcal{Q}}\right)^2\right.\\ &\quad + \frac{1}{\beta_3}\left(\frac{\partial\alpha_1}{\partial\dot{\mathcal{Q}}}\ddot{\mathcal{Q}}\right)^2 + \frac{1}{\beta_4}\left(\frac{\partial\alpha_1}{\partial y_r}\dot{y}_r\right)^2\\ &\quad \left.+ \frac{1}{\beta_5}\left(\frac{\partial\alpha_1}{\partial\dot{y}_r}\ddot{y}_r\right)^2 + \frac{1}{\gamma}\right) + \frac{\gamma\sigma_B^2}{4} + \frac{\sum_{i=1}^5\beta_i}{4}\end{aligned} \tag{58}$$

Authorized licensed use limited to: GUANGZHOU UNIVERSITY. Downloaded on November 21,2024 at 07:08:04 UTC from IEEE Xplore. Restrictions apply.

Hence, the dynamic $\dot{V}_2$ satisfies

$$\dot{V}_2 \le \eta_2\hat{\Xi}(\xi_1,\xi_2,t)+\frac{\gamma\sigma_B^2}{4}+\frac{\sum_{i=1}^5\beta_i}{4} + \eta_2^2\left(\frac{1}{\beta_1}\left(\frac{\partial\alpha_1}{\partial\xi_1}\xi_2\right)^2+\frac{1}{\beta_2}\left(\frac{\partial\alpha_1}{\partial\mathcal{Q}}\dot{\mathcal{Q}}\right)^2+\frac{1}{\beta_3}\left(\frac{\partial\alpha_1}{\partial\dot{\mathcal{Q}}}\ddot{\mathcal{Q}}\right)^2 + \frac{1}{\beta_4}\left(\frac{\partial\alpha_1}{\partial y_r}\dot{y}_r\right)^2+\frac{1}{\beta_5}\left(\frac{\partial\alpha_1}{\partial\dot{y}_r}\ddot{y}_r\right)^2+\frac{1}{\gamma}\right)+\eta_2\bar{\mathcal{S}}^{-1}u \quad (59)$$

Choosing the following Lyapunov function V in *Step 2*

$$V = V_1 + V_2 \quad (60)$$

Consequently, we obtain from the derivative of V_1 in (54) and V_2 dynamic in (59) that

$$\dot{V} = \dot{V}_1 + \dot{V}_2 \le -\rho_1\eta_1^2+\frac{1}{\iota_3}\chi_1^2\eta_1^2\eta_2^2+\frac{\sum_{i=1}^3\iota_i}{4} + \eta_2\hat{\Xi}(\xi_1,\xi_2,t)+\frac{\gamma\sigma_B^2}{4}+\frac{\sum_{i=1}^5\beta_i}{4} + \eta_2^2\left(\frac{1}{\beta_1}\left(\frac{\partial\alpha_1}{\partial\xi_1}\xi_2\right)^2+\frac{1}{\beta_2}\left(\frac{\partial\alpha_1}{\partial\mathcal{Q}}\dot{\mathcal{Q}}\right)^2+\frac{1}{\beta_3}\left(\frac{\partial\alpha_1}{\partial\dot{\mathcal{Q}}}\ddot{\mathcal{Q}}\right)^2 + \frac{1}{\beta_4}\left(\frac{\partial\alpha_1}{\partial y_r}\dot{y}_r\right)^2+\frac{1}{\beta_5}\left(\frac{\partial\alpha_1}{\partial\dot{y}_r}\ddot{y}_r\right)^2+\frac{1}{\gamma}\right)+\eta_2\bar{\mathcal{S}}^{-1}u \quad (61)$$

Substituting the proposed approximation-free actual control input u in (45) into (51), it holds that

$$\dot{V} \le -\rho_1\eta_1^2+\frac{1}{\iota_3}\chi_1^2\eta_1^2\eta_2^2+\frac{\sum_{i=1}^3\iota_i}{4} + \frac{\gamma\sigma_B^2}{4}+\frac{\sum_{i=1}^5\beta_i}{4}+\eta_2\hat{\Xi}(\xi_1,\xi_2,t) + \eta_2^2\left(\frac{1}{\beta_1}\left(\frac{\partial\alpha_1}{\partial\xi_1}\xi_2\right)^2+\frac{1}{\beta_2}\left(\frac{\partial\alpha_1}{\partial\mathcal{Q}}\dot{\mathcal{Q}}\right)^2+\frac{1}{\beta_3}\left(\frac{\partial\alpha_1}{\partial\dot{\mathcal{Q}}}\ddot{\mathcal{Q}}\right)^2 + \frac{1}{\beta_4}\left(\frac{\partial\alpha_1}{\partial y_r}\dot{y}_r\right)^2+\frac{1}{\beta_5}\left(\frac{\partial\alpha_1}{\partial\dot{y}_r}\ddot{y}_r\right)^2+\frac{1}{\gamma}\right) + \eta_2\bar{\mathcal{S}}^{-1}\left(\bar{\mathcal{S}}\left(-\rho_2\eta_2-\hat{\Xi}(\xi_1,\xi_2,t)-\frac{1}{\iota_3}\chi_1^2\eta_1^2\eta_2^2-\frac{\eta_2}{\gamma} - \frac{\eta_2}{\beta_1}\left(\frac{\partial\alpha_1}{\partial\xi_1}\xi_2\right)^2-\frac{\eta_2}{\beta_2}\left(\frac{\partial\alpha_1}{\partial\mathcal{Q}}\dot{\mathcal{Q}}\right)^2-\frac{\eta_2}{\beta_3}\left(\frac{\partial\alpha_1}{\partial\dot{\mathcal{Q}}}\ddot{\mathcal{Q}}\right)^2 - \frac{\eta_2}{\beta_4}\left(\frac{\partial\alpha_1}{\partial y_r}\dot{y}_r\right)^2-\frac{\eta_2}{\beta_5}\left(\frac{\partial\alpha_1}{\partial\dot{y}_r}\ddot{y}_r\right)^2\right)\right) \quad (62)$$

As a result, the following holds

$$\dot{V} \le -\rho_1\eta_1^2+\frac{1}{\iota_3}\chi_1^2\eta_1^2\eta_2^2+\frac{\sum_{i=1}^3\iota_i}{4}+\frac{\gamma\sigma_B^2}{4}+\frac{\sum_{i=1}^5\beta_i}{4} + \eta_2^2\left(\frac{1}{\beta_1}\left(\frac{\partial\alpha_1}{\partial\xi_1}\xi_2\right)^2+\frac{1}{\beta_2}\left(\frac{\partial\alpha_1}{\partial\mathcal{Q}}\dot{\mathcal{Q}}\right)^2+\frac{1}{\beta_3}\left(\frac{\partial\alpha_1}{\partial\dot{\mathcal{Q}}}\ddot{\mathcal{Q}}\right)^2 + \frac{1}{\beta_4}\left(\frac{\partial\alpha_1}{\partial y_r}\dot{y}_r\right)^2+\frac{1}{\beta_5}\left(\frac{\partial\alpha_1}{\partial\dot{y}_r}\ddot{y}_r\right)^2+\frac{1}{\gamma}\right)+\eta_2\hat{\Xi}(\xi_1,\xi_2,t) - \eta_2\hat{\Xi}(\xi_1,\xi_2,t)-\rho_2\eta_2^2-\frac{1}{\iota_3}\chi_1^2\eta_1^2\eta_2^2+\eta_2 \times\left(-\frac{1}{\beta_1}\left(\frac{\partial\alpha_1}{\partial\xi_1}\xi_2\right)^2-\frac{1}{\beta_2}\left(\frac{\partial\alpha_1}{\partial\mathcal{Q}}\dot{\mathcal{Q}}\right)^2-\frac{1}{\beta_3}\left(\frac{\partial\alpha_1}{\partial\dot{\mathcal{Q}}}\ddot{\mathcal{Q}}\right)^2 - \frac{1}{\beta_4}\left(\frac{\partial\alpha_1}{\partial y_r}\dot{y}_r\right)^2-\frac{1}{\beta_5}\left(\frac{\partial\alpha_1}{\partial\dot{y}_r}\ddot{y}_r\right)^2-\frac{1}{\gamma}\right) \le -\rho_1\eta_1^2-\rho_2\eta_2^2+\frac{\sum_{i=1}^3\iota_i}{4}+\frac{\gamma\sigma_B^2}{4}+\frac{\sum_{i=1}^5\beta_i}{4} \quad (63)$$

The dynamic of V in (63) can be rewritten as

$$\dot{V} \le -\mathcal{G}V + \mathcal{E}$$

where $\mathcal{G} := \min\{\rho_1,\rho_2\}$ and $\mathcal{E} := \frac{\sum_{i=1}^3\iota_i}{4}+\frac{\gamma\sigma_B^2}{4}+\frac{\sum_{i=1}^5\beta_i}{4}$. Therefore, the stability [21] of the closed-loop system is proved. This concludes that the transformed error signals η_1 and η_2 in (30) and (38) are bounded, namely,

$$\eta_1,\eta_2 \in L_\infty, \text{ for } \forall t \ge 0$$

This implies that

$$-\mathcal{Q}(t) < e_1 < \mathcal{Q}(t) \quad (64)$$

Next, proof of (64) is provided. If (64) is violated in time instant t_c with $t_c > 0$, namely, $e_1(t_c) \ge \mathcal{Q}(t_c)$ or $e_1(t_c) \le -\mathcal{Q}(t_c)$. Define $\mathcal{H}(t) := \frac{e_1(t)}{\mathcal{Q}(t)}$, $\mathcal{H}(t_c) \ge 1$ or $\mathcal{H}(t_c) \le -1$ holds in this case. According to the fixed point theorem [32] of continuous functions, there exist a time instant t_m with $t_m \in (0,t_c)$, such that $\mathcal{H}(t_m) = 1$ or $\mathcal{H}(t_m) = -1$ holds. Accordingly, from (30) and (31), it concludes that $\mathcal{D}(t_m) = 0$ and $\eta_1(t_m) = \infty$. However, by using the proposed control scheme (41) and (45), $\eta_1 \in L_\infty$ is proved as detailed above. Thus, $-\mathcal{Q}(t) < e_1(t) < \mathcal{Q}(t)$ holds for $t > 0$. Because the initial error $e_1(0)$ is finite, and $\mathcal{Q}(t) = \infty$ when $t = 0$, therefore, (64) holds for $t = 0$. In summary, (64) holds for $t \ge 0$. The proof of *Theorem 1* is complete.

By embedding the proposed controller (45), the stability of the sprung underactuated subsystem, consisting of x_s and $\dot{x}_s$, is proved and analyzed above. The suspension system (5) is a fourth-order nonlinear system that is composed of the sprung subsystem and the unsprung subsystem. The unsprung internal subsystem, namely the zero dynamics system [7], [16], consists of x_u and $\dot{x}_u$. The stability of the zero dynamics subsystem [7], [16] has been thoroughly analyzed and proved in the existing results, and the detailed analysis and stability proof can be found in [7] and [16].

Remark 1: Unlike [8] which switches circuits according to operating states for reducing energy consumption, bionic dynamics do not change the hardware structures of suspension to achieve energy savings in a simple and effective way. By embedding transformation functions into the developed controller, the error signal is bounded and converges to a neighborhood of 0 after a prespecified time. Moreover, the time delay information allows us to handle actuator faults, uncertainties, and disturbances without approximation mechanisms [33]. Meanwhile, the developed control scheme also can be applied to other electromechanical systems such as vehicle longitudinal dynamics [34], one-link manipulators, ship course changing, pendulum systems, etc.

IV. Experiments

The experimental results are provided in this section to illustrate the effectiveness and benefits accomplished by the

Authorized licensed use limited to: GUANGZHOU UNIVERSITY. Downloaded on November 21,2024 at 07:08:04 UTC from IEEE Xplore. Restrictions apply.

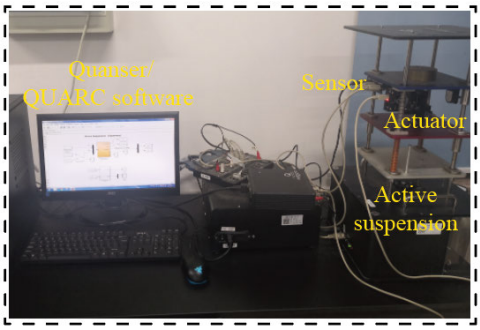

Fig. 3. AS experimental setup.

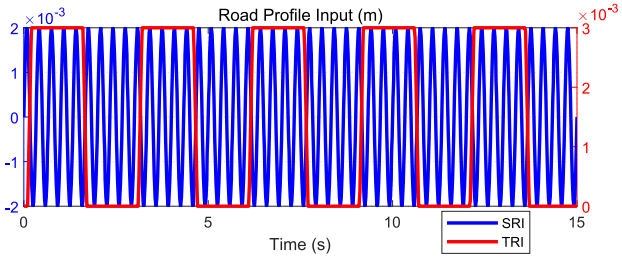

Fig. 4. Road inputs.

TABLE I
PARAMETER SETTINGS OF BIONIC REFERENCE DYNAMICS

Parameter	Value(Unit)	Parameter	Value(Unit)
M_b	$3kg$	λ_1	$5N \cdot s \cdot m^{-1}$
θ_l	$\frac{\pi}{6} rad$	λ_1	$0.15N \cdot s \cdot m^{-1}$
p_0	$500N \cdot m^{-1}$	w_l	$0.1m$
p_1	$350N \cdot m^{-1}$	w_r	$0.2m$

developed control scheme. The AS experimental apparatus [7] is shown in Fig. 3. The displacements and acceleration of the experimental platform are measured with high-precision encoders and accelerometer. The computer calculates the control inputs with Quanser according to the real-time states via data acquisition equipment through analog-to-digital conversion. The control inputs are transferred to the motor via digital-to-analog conversion to control the active suspension.

For comparison purposes, the sinusoidal road input (SRI) and trapezoidal road input (TRI) [25] plotted in Fig. 4 are used as road excitations to test the controller performance. Meanwhile, the finite-time estimator-based adaptive controller (FEAC) [25] is performed to compare with the proposed control method. The bionic suspension parameter settings with $q_n = 4$ are shown in Table I. The actuator faults are set as $\zeta(t) = 0.76 + 0.05 \times sin(t)$ and $\zeta_b = 0.08$. The specific parameter settings of the corresponding controllers are

- Passive: passive suspension.
- FEAC [25]: The controller parameters are chosen as $k_1 = 29.9$, $k_2 = 30.1$, $\lambda_0 = 2.98$, $\lambda_1 = 1.51$, $\lambda_2 = 1.09$, $\lambda_3 = 1.49$, $\lambda_4 = 1.1$, $L_1 = 149.9$, $L_2 = 20.1$, $\eta_1 = 9.9$, $\eta_2 = 9.9$. The parameter symbols and controller structure remain the same as [25].
- Proposed: The constructed controller (45) with $\mathcal{L} = 2$, $\iota_3 = 1$, $\mathcal{Q}_\varrho = 5 \times 10^{-3}$, γ =1, $\bar{\mathcal{S}} = 1$, $\beta_1 = 1$, $T_\zeta = 10$, $\mathcal{R}_s = 1 \times 10^{-3}$, $\beta_2 = 1$, $\beta_3 = 1$, $\kappa = 3 \times 10^3$, $\beta_4 = 1$, $\rho_1 = 3$, $\beta_5 = 1$, $\rho_2 = 1 \times 10^3$ is used to perform experiments.

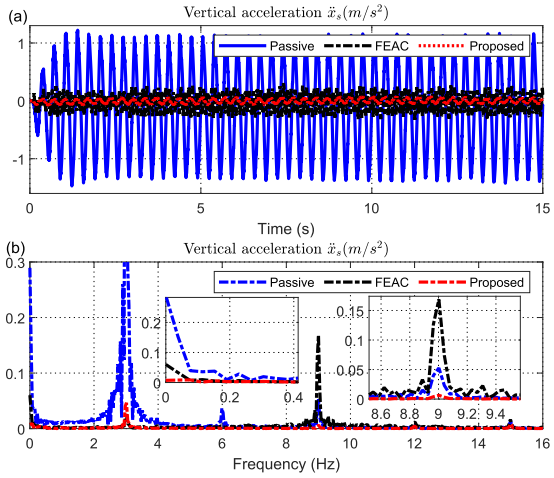

Fig. 5. The time-domain and frequency-domain vibration responses of the sprung mass under SRI.

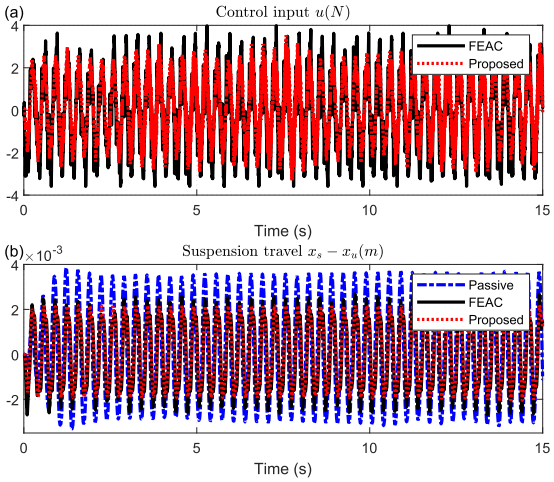

Fig. 6. The control inputs and suspension travels under SRI.

The vertical acceleration responses of the sprung mass m_0 at the time domain and the frequency domain under SRI are plotted in Fig. 5(a) and (b), respectively. It can be observed from Fig. 5(a) that the proposed prespecified time control scheme, compared to the passive suspension and FEAC [25], can effectively isolate vertical vibration even with time-varying actuator faults, which implies superior reliability and ride comfort. Meanwhile, from the frequency domain acceleration responses in Fig. 5(b), the constructed prespecified time controller achieves similar ride comfort improvement.

The corresponding control inputs and suspension travels are illustrated in Fig. 6(a) and (b). By employing the presented prespecified controller, compared with FEAC [25], better control performance is obtained with smaller control magnitude. This means that energy consumption is reduced significantly.

To further evaluate the performance quantitatively, the root mean square (RMS) [35] of the sprung vibration acceleration and the energy consumption $\mathcal{C}_+$ [36] are calculated and

Authorized licensed use limited to: GUANGZHOU UNIVERSITY. Downloaded on November 21,2024 at 07:08:04 UTC from IEEE Xplore. Restrictions apply.

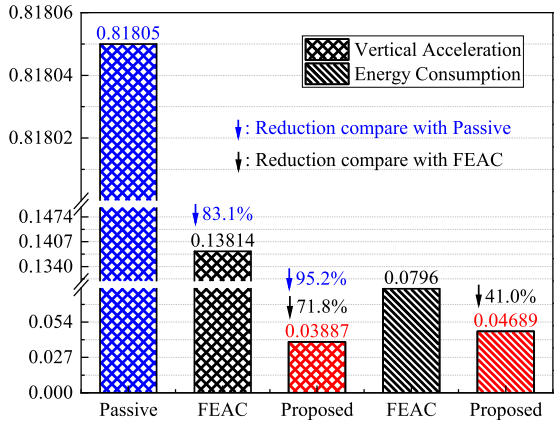

Fig. 7. Quantitative comparative results under SRI.

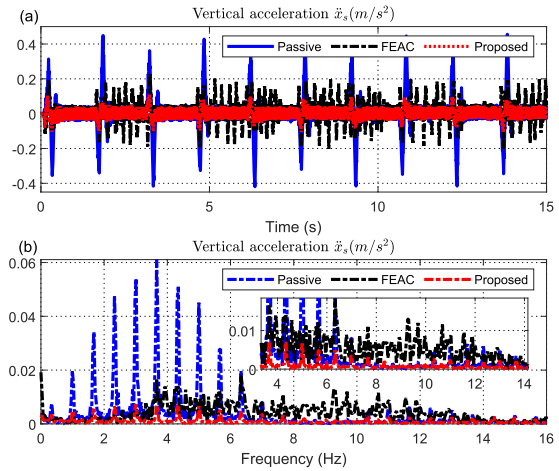

Fig. 8. The vertical acceleration responses of the sprung mass under TRI.

visualized in Fig. 7. The RMS and energy consumption can be calculated as below

$$\mathrm{RMS}_{\nu} = \sqrt{\frac{1}{\mathcal{A}}\int_0^{\mathcal{A}} \nu^T(t)\nu(t)dt} \tag{65}$$

$$\mathcal{C}_+(t) = \begin{cases} u(t)\big(\dot{x}_s - \dot{x}_u\big), & \text{if } u(t)\big(\dot{x}_s - \dot{x}_u\big) > 0 \\ 0, & \text{else} \end{cases} \tag{66}$$

where $\nu(t)$ represents the state signal and $\mathcal{A}$ is the total time. x_s, x_u and $u(t)$ are defined above. $\mathcal{C}_+(t)$ denotes energy consumption. Compared to the passive suspension, vehicle vertical vibration is suppressed significantly ($\mathrm{RMS}_{\ddot{x}_s}$ is reduced by over 95%). Moreover, the comfort performance and energy-saving characteristics compared to FEAC [25] are further improved ($\mathrm{RMS}_{\ddot{x}_s}$ is reduced by over 70% and $\mathrm{RMS}_{\mathcal{C}_+}$ is reduced by over 40%).

To adequately validate the designed controller, the trapezoidal road excitation in Fig. 4 is introduced for further verification. The selected controller parameters and time-varying actuator faults settings are the same as in the SRI test scenario. As shown in Fig. 8(a), the sprung acceleration time-domain responses still can be suppressed by the developed prespecified time reliable controller under time-varying actuator faults. Moreover, the corresponding frequency

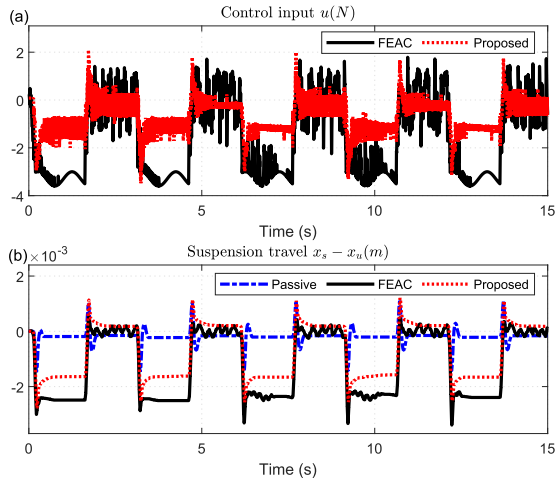

Fig. 9. The control inputs and suspension travels under TRI.

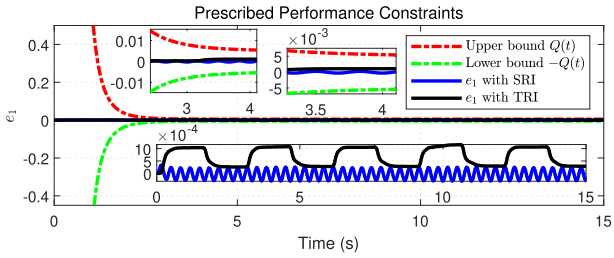

Fig. 10. Transient behaviors of the tracking error e_1 with SRI and TRI.

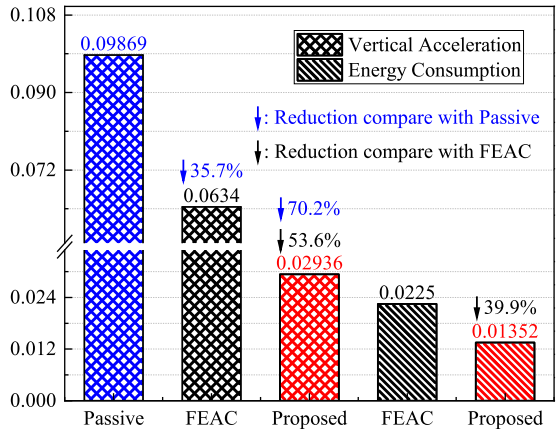

Fig. 11. Quantitative comparative results under TRI.

domain responses, both in the low and high-frequency regions, are reduced considerably as in Fig. 8(b) compared to the passive suspension and FEAC [25].

The control inputs of FEAC [25] and the developed controller are provided in Fig. 9(a), while the corresponding suspension travels are plotted in Fig. 9(b). It is obvious that both the controller magnitude and the suspension travel are reduced by using the proposed controller compared to FEAC [25]. Meanwhile, the transient behaviors of the tracking error e_1 under SRI and TRI are shown in Fig. 10. It can be observed the tracking error e_1 satisfies the designed performance constraints, namely $e_1 \in (-\mathcal{Q}(t), \mathcal{Q}(t))$, which is in agreement with the proof and analysis of *Theorem 1*.

Authorized licensed use limited to: GUANGZHOU UNIVERSITY. Downloaded on November 21,2024 at 07:08:04 UTC from IEEE Xplore. Restrictions apply.

Similar to SRI, the RMS (65) of sprung acceleration and energy consumption (66) are calculated quantitatively and reported in Fig. 11. The RMS reduction in sprung acceleration for the proposed control method is over 70% and 50% compared with the passive suspension and FEAC [25], respectively. Moreover, compared to FEAC [25], the energy consumption of the proposed controller is reduced by about 40%. By employing the developed control scheme, superior energy saving is achieved while ride comfort is enhanced.

V. Conclusion

In this paper, a prespecified time energy-efficient fault-tolerant controller is presented. By using the elaborately designed control structure, the suspension states can converge to a neighborhood of 0 in a prespecified finite time interval, which is independent of the controller parameters and initial states. Actuator faults, external disturbances, and uncertainties, including model uncertainty and parameter uncertainty, can be handled elegantly by introducing time delay information. Meanwhile, the vertical vibration and energy consumption of AS are suppressed significantly. Experimental results under SRI and TRI demonstrate that the proposed controller can achieve excellent ride comfort and energy-saving property. Specifically, the reduction in $\mathrm{RMS}_{\ddot{x}_s}$ compared to the passive suspension is more than 70%. Compared to FEAC [25], the $\mathrm{RMS}_{\ddot{x}_s}$ is reduced by over 50% while energy consumption RMS_{C_+} is reduced by approximately 40%.

Future work attempts to further address sensor failures to improve reliability and focus on achieving prespecified time zero error stabilization to enhance control performance. By using visual information, trying to combine the advanced control method with the motion planning [34] layer of autonomous vehicles [37], including combining path planning to bypass uneven road excitation to improve ride comfort, and employing speed planning to optimize the multi-objective performance, is also an interesting topic.

References

[1] R. Krtolica and D. Hrovat, "Optimal active suspension control based on a half-car model: An analytical solution," *IEEE Trans. Autom. Control*, vol. 37, no. 4, pp. 528–532, Apr. 1992.

[2] H. Pan, W. Sun, H. Gao, and X. Jing, "Disturbance observer-based adaptive tracking control with actuator saturation and its application," *IEEE Trans. Autom. Sci. Eng.*, vol. 13, no. 2, pp. 868–875, Apr. 2016.

[3] M. Zhang and X. Jing, "A bioinspired dynamics-based adaptive fuzzy SMC method for half-car active suspension systems with input dead zones and saturations," *IEEE Trans. Cybern.*, vol. 51, no. 4, pp. 1743–1755, Apr. 2021.

[4] H. Pan, X. Jing, W. Sun, and H. Gao, "A bioinspired dynamics-based adaptive tracking control for nonlinear suspension systems," *IEEE Trans. Control Syst. Technol.*, vol. 26, no. 3, pp. 903–914, May 2018.

[5] D. Lee, S. Jin, and C. Lee, "Deep reinforcement learning of semi-active suspension controller for vehicle ride comfort," *IEEE Trans. Veh. Technol.*, vol. 72, no. 1, pp. 327–339, Jan. 2023.

[6] Y. Li, S. Ma, K. Li, and S. Tong, "Adaptive fuzzy output feedback fault-tolerant control for active suspension systems," *IEEE Trans. Intell. Vehicles*, early access, May 3, 2023, doi: 10.1109/TIV.2023.3272529.

[7] T. Huang, J. Wang, and H. Pan, "Adaptive bioinspired preview suspension control with constrained velocity planning for autonomous vehicles," *IEEE Trans. Intell. Vehicles*, vol. 8, no. 7, pp. 3925–3935, Jul. 2023.

[8] S. Yan and W. Sun, "Self-powered suspension criterion and energy regeneration implementation scheme of motor-driven active suspension," *Mech. Syst. Signal Process.*, vol. 94, pp. 297–311, Sep. 2017.

[9] M. Gaggero and L. Caviglione, "Model predictive control for energy-efficient, quality-aware, and secure virtual machine placement," *IEEE Trans. Autom. Sci. Eng.*, vol. 16, no. 1, pp. 420–432, Jan. 2019.

[10] H. Nazemian and M. Masih-Tehrani, "Development of an optimized game controller for energy saving in a novel interconnected air suspension system," *Proc. Inst. Mech. Eng., D, J. Automobile Eng.*, vol. 234, no. 13, pp. 3068–3080, Nov. 2020.

[11] Z. Wu, X. Jing, J. Bian, F. Li, and R. Allen, "Vibration isolation by exploring bio-inspired structural nonlinearity," *Bioinspiration Biomimetics*, vol. 10, no. 5, Oct. 2015, Art. no. 056015.

[12] J. Bian and X. Jing, "Superior nonlinear passive damping characteristics of the bio-inspired limb-like or X-shaped structure," *Mech. Syst. Signal Process.*, vol. 125, pp. 21–51, Jun. 2019.

[13] X. Feng, X. Jing, Z. Xu, and Y. Guo, "Bio-inspired anti-vibration with nonlinear inertia coupling," *Mech. Syst. Signal Process.*, vol. 124, pp. 562–595, Jun. 2019.

[14] D. Hrovat, "Survey of advanced suspension developments and related optimal control applications," *Automatica*, vol. 33, no. 10, pp. 1781–1817, 1997.

[15] H. Li, X. Jing, and H. R. Karimi, "Output-feedback-based H_∞ control for vehicle suspension systems with control delay," *IEEE Trans. Ind. Electron.*, vol. 61, no. 1, pp. 436–446, Jan. 2014.

[16] H. Pan and W. Sun, "Nonlinear output feedback finite-time control for vehicle active suspension systems," *IEEE Trans. Ind. Informat.*, vol. 15, no. 4, pp. 2073–2082, Apr. 2019.

[17] T. Yang and J. Dong, "Predefined-time adaptive fault-tolerant control for switched odd-rational-power multi-agent systems," *IEEE Trans. Autom. Sci. Eng.*, early access, Oct. 10, 2022, doi: 10.1109/TASE.2022.3208029.

[18] A. Garza-Alonso, M. Basin, and P. C. Rodriguez-Ramirez, "Predefined-time backstepping stabilization of autonomous nonlinear systems," *IEEE/CAA J. Autom. Sinica*, vol. 9, no. 11, pp. 2020–2022, Nov. 2022.

[19] H. Ye and Y. Song, "Prescribed-time tracking control of MIMO nonlinear systems under non-vanishing uncertainties," *IEEE Trans. Autom. Control*, vol. 68, no. 6, pp. 3664–3671, Jun. 2023.

[20] Y. Cao, J. Cao, and Y. Song, "Practical prescribed time tracking control over infinite time interval involving mismatched uncertainties and non-vanishing disturbances," *Automatica*, vol. 136, Feb. 2022, Art. no. 110050.

[21] Y. Li, T. Wang, W. Liu, and S. Tong, "Neural network adaptive output-feedback optimal control for active suspension systems," *IEEE Trans. Syst., Man, Cybern., Syst.*, vol. 52, no. 6, pp. 4021–4032, Jun. 2022.

[22] S. Roshanravan and S. Shamaghdari, "Adaptive fault-tolerant tracking control for affine nonlinear systems with unknown dynamics via reinforcement learning," *IEEE Trans. Autom. Sci. Eng.*, early access, Dec. 20, 2022, doi: 10.1109/TASE.2022.3223702.

[23] H. Li, Y. Wu, and M. Chen, "Adaptive fault-tolerant tracking control for discrete-time multiagent systems via reinforcement learning algorithm," *IEEE Trans. Cybern.*, vol. 51, no. 3, pp. 1163–1174, Mar. 2021.

[24] T. Huang, J. Wang, H. Pan, and W. Sun, "Finite-time fault-tolerant integrated motion control for autonomous vehicles with prescribed performance," *IEEE Trans. Transport. Electrific.*, early access, Dec. 26, 2022, doi: 10.1109/TTE.2022.3232521.

[25] X. Guo, J. Zhang, and W. Sun, "Robust saturated fault-tolerant control for active suspension system via partial measurement information," *Mech. Syst. Signal Process.*, vol. 191, May 2023, Art. no. 110116.

[26] Y. Li, F. Qu, and S. Tong, "Observer-based fuzzy adaptive finite-time containment control of nonlinear multiagent systems with input delay," *IEEE Trans. Cybern.*, vol. 51, no. 1, pp. 126–137, Jan. 2021.

[27] F. Jia, J. Huang, and X. He, "Predefined-time fault-tolerant control for a class of nonlinear systems with actuator faults and unknown mismatched disturbances," *IEEE Trans. Autom. Sci. Eng.*, early access, Jun. 26, 2023, doi: 10.1109/TASE.2023.3286663.

[28] H. Pan, C. Zhang, and W. Sun, "Fault-tolerant multiplayer tracking control for autonomous vehicle via model-free adaptive dynamic programming," *IEEE Trans. Rel.*, early access, Sep. 30, 2022, doi: 10.1109/TR.2022.3208467.

[29] P. Krishnamurthy, F. Khorrami, and M. Krstic, "A dynamic high-gain design for prescribed-time regulation of nonlinear systems," *Automatica*, vol. 115, May 2020, Art. no. 108860.

Authorized licensed use limited to: GUANGZHOU UNIVERSITY. Downloaded on November 21,2024 at 07:08:04 UTC from IEEE Xplore. Restrictions apply.

[30] H. M. Becerra, C. R. Vázquez, G. Arechavaleta, and J. Delfin, "Predefined-time convergence control for high-order integrator systems using time base generators," *IEEE Trans. Control Syst. Technol.*, vol. 26, no. 5, pp. 1866–1873, Sep. 2018.

[31] M. Jin, J. Lee, P. Hun Chang, and C. Choi, "Practical nonsingular terminal sliding-mode control of robot manipulators for high-accuracy tracking control," *IEEE Trans. Ind. Electron.*, vol. 56, no. 9, pp. 3593–3601, Sep. 2009.

[32] V. Kostrykin and A. Oleynik, "An intermediate value theorem for monotone operators in ordered Banach spaces," *Fixed Point Theory Appl.*, vol. 2012, no. 1, pp. 1–4, Dec. 2012.

[33] H. Li, Y. Wu, M. Chen, and R. Lu, "Adaptive multigradient recursive reinforcement learning event-triggered tracking control for multiagent systems," *IEEE Trans. Neural Netw. Learn. Syst.*, vol. 34, no. 1, pp. 144–156, Jan. 2023.

[34] T. Huang, H. Pan, W. Sun, and H. Gao, "Sine resistance network-based motion planning approach for autonomous electric vehicles in dynamic environments," *IEEE Trans. Transport. Electrific.*, vol. 8, no. 2, pp. 2862–2873, Jun. 2022.

[35] N. Z. Gebraeel and M. A. Lawley, "A neural network degradation model for computing and updating residual life distributions," *IEEE Trans. Autom. Sci. Eng.*, vol. 5, no. 1, pp. 154–163, Jan. 2008.

[36] M. Zhang, X. Jing, and G. Wang, "Bioinspired nonlinear dynamics-based adaptive neural network control for vehicle suspension systems with uncertain/unknown dynamics and input delay," *IEEE Trans. Ind. Electron.*, vol. 68, no. 12, pp. 12646–12656, Dec. 2021.

[37] H. Pan, Y. Hong, W. Sun, and Y. Jia, "Deep dual-resolution networks for real-time and accurate semantic segmentation of traffic scenes," *IEEE Trans. Intell. Transp. Syst.*, vol. 24, no. 3, pp. 3448–3460, Mar. 2023.

Tenglong Huang (Graduate Student Member, IEEE) received the B.E. degree in automation from the Henan University of Technology, Zhengzhou, China, in 2019. He is currently pursuing the Ph.D. degree with the Research Institute of Intelligent Control and Systems, Harbin Institute of Technology, Harbin, China.

His current research interests include motion planning, vehicle dynamics control, adaptive control, fault-tolerant control, and intelligent vehicles.

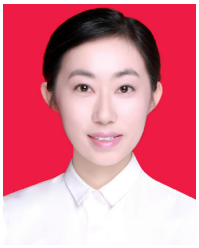

Jue Wang received the B.S. degree in automation and the M.S. degree in pattern recognition and intelligent systems from Huaqiao University, Xiamen, China, in 2016 and 2019, respectively, and the Ph.D. degree from the Harbin Institute of Technology, Harbin, China, in 2023.

She is currently a Post-Doctoral Fellow with Ningbo Institute of Intelligent Equipment Technology Company Ltd., Ningbo, China, and the University of Science and Technology of China, Hefei, China. Her current research interests include adaptive control, fault-tolerant control, mechatronics, and intelligent vehicles.

Huihui Pan (Senior Member, IEEE) received the Ph.D. degree in control science and engineering from the Harbin Institute of Technology, Harbin, China, in 2017, and the Ph.D. degree in mechanical engineering from The Hong Kong Polytechnic University, Hong Kong, in 2018.

Since December 2017, he has been with the Research Institute of Intelligent Control and Systems, Harbin Institute of Technology. His current research interests include nonlinear control, vehicle dynamic control, and intelligent vehicles.

Dr. Pan is an Associate Editor of IEEE TRANSACTIONS ON SYSTEMS, MAN, AND CYBERNETICS: SYSTEMS, IEEE TRANSACTIONS ON INTELLIGENT VEHICLES, and *Mechatronics*.

Authorized licensed use limited to: GUANGZHOU UNIVERSITY. Downloaded on November 21,2024 at 07:08:04 UTC from IEEE Xplore. Restrictions apply.